Shallow Water Equations

Blair Emanuel, Kevin McClure, Patrick Varin

1 Introduction

The shallow water equations are a set of partial differential equations that model fluid waves. They are so named because the simplification that bridges these equations with first principles assumes that the water is shallow in relation to the wavelength of the waves.

The most famous application of the shallow water equations is in tsunami modelling where the wavelengths in question are large even compared to the depth of the ocean. Tsunami models that implement the shallow water equations allow predictions for the propagation speed of waves and the energy of these waves as they reach the shore. In addition to tsunami models, these equations have applications in risk assessment for floods, and in hydraulic engineering to determine the integrity of load-bearing structures. They can also serve as predictive tools to calculate stresses on river beds and they have ecological applications in erosion prediction.

Here we will consider numerical methods to approximating solutions to the shallow water equations over arbitrarily defined domains consisting of shoreline boundaries as well as an irregular topography below the surface of the water and external stresses on the surface of the water, such as wind. These solutions will allow us to simulate and analyze, in detail, a case study of a dam as it bursts resulting in the violent flow of water.

2 Derivation of the Shallow Water Equations in Two Dimensions

The shallow water wave equations can be derived from the Navier Stoke's Equations for an incompressible fluid (Equations 1) with a few simplifying assumptions. In this case gravity will be considered the only body force acting on the fluid, ignoring Coriolis forces.

$$\nabla \cdot \vec{v} = 0 \tag{1a}$$

$$\frac{\partial}{\partial t}\rho\vec{v} + \nabla \cdot (\rho\vec{v}\vec{v}) = -\nabla P + \rho\vec{g} + \nabla \cdot T \tag{1b}$$

In this case $\vec{v}$ is the velocity field of the fluid, $\vec{g}$ is the acceleration of gravity, ρ is the density of the fluid and P is the pressure in the fluid, both scalar fields, while T is the stress tensor field acting on the fluid. The contribution of the stress tensor field will be important in modeling the effect of wind on the surface of the water. For now this will be ignored but it is included in a later derivation.

Expanding the differential operators in Equation 1 allows a closer inspection of the individual elements of the velocity components, $\vec{v} = \begin{pmatrix} u \\ v \\ w \end{pmatrix}$, and yields the Navier Stokes equations in the form;

$$\frac{\partial u}{\partial x} + \frac{\partial v}{\partial y} + \frac{\partial w}{\partial z} = 0 \tag{2a}$$

$$\frac{\partial(\rho u)}{\partial t} + \frac{\partial(\rho u^2)}{\partial x} + \frac{\partial(\rho uv)}{\partial y} + \frac{\partial(\rho uw)}{\partial z} = -\frac{\partial P}{\partial x} \tag{2b}$$

$$\frac{\partial(\rho v)}{\partial t} + \frac{\partial(\rho uv)}{\partial x} + \frac{\partial(\rho v^2)}{\partial y} + \frac{\partial(\rho vw)}{\partial z} = -\frac{\partial P}{\partial y} \tag{2c}$$

$$\frac{\partial(\rho w)}{\partial t} + \frac{\partial(\rho uw)}{\partial x} + \frac{\partial(\rho wv)}{\partial y} + \frac{\partial(\rho w^2)}{\partial z} = -\frac{\partial P}{\partial z} - \rho g \tag{2d}$$

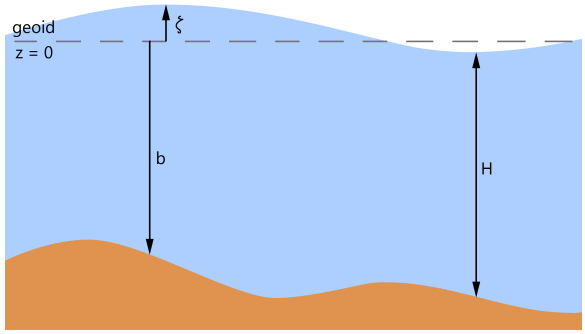

Fig. 1. Naming conventions for dimensions in the z direction.

For our calculations, we will adopt the naming conventions shown in Figure 1. The height of the top and bottom surfaces are given in reference to the geoid, the equilibrium level of the water. The surface of the water is given by $z = \zeta$, a positive measurement above the geoid. The bathymetry, geometry of the bottom surface, is given by $z = -b$, where b is a positive value below the geoid. These sign conventions allow us to express the total height of the water, H, as the sum $H = \zeta + b$.

At the bottom surface of the body of water, there is a no slip condition (Equation 3a) since the bottom is stationary and no flow perpendicular to the bottom (Equation 3b). The water is free to flow on the top surface, but there is no relative normal flow across the surface (Equation 4a). Additionally, the atmospheric pressure at the surface of the water is assumed to be zero (Equation 4b) to simplify the calculations.

(at z = b)

$$v = u = 0 \tag{3a}$$

$$u\frac{\partial b}{\partial x} + v\frac{\partial b}{\partial y} + w = 0 \tag{3b}$$

(at z = ζ)

$$\frac{\partial \zeta}{\partial t} + u\frac{\partial \zeta}{\partial x} + v\frac{\partial \zeta}{\partial y} - w = 0 \tag{4a}$$

$$P_{atm} = 0 \tag{4b}$$

Since we are dealing with "shallow" water, all of the terms in the z component equation except for pressure and gravity are small and therefore can be ignored. The resulting equation (Equation 5) can be solved for pressure in terms of the water's depth (Equation 6). This can then be differentiated with respect to x and y to determine the pressure gradient in the lateral directions (Equation 7).

$$0 = -\frac{\partial P}{\partial z} + \rho g \tag{5}$$

$$P = \rho g(\zeta - z) \tag{6}$$

$$\frac{\partial P}{\partial x} = \rho g \frac{\partial \zeta}{\partial x} \tag{7a}$$

$$\frac{\partial P}{\partial y} = \rho g \frac{\partial \zeta}{\partial y} \tag{7b}$$

To calculate the total mass in the system, the equation for conservation of mass is integrated from $z = -b$ to $z = \zeta$ (Equation 8). The limits vary with position and time, therefore the Liebniz Rule is used (see appendix for detailed calculations) and boundary conditions are applied. Two of the remaining integrals can be changed into average values using the equation $\bar{u} = \frac{1}{H}\int_{-b}^{\zeta} u dz$, with a similar equation for the y velocity. After changing the velocities to averages, the no relative normal flow condition is applied and substituted into the equation to yield the final equation for conservation of mass (Equation 9).

$$0 = \int_{-b}^{\zeta} \nabla \cdot \vec{v} dv \tag{8}$$

$$\frac{\partial H}{\partial t} + \frac{\partial \bar{u} H}{\partial x} + \frac{\partial \bar{v} H}{\partial y} = 0 \tag{9}$$

Similar to the conservation of mass equation, the momentum equations are divided by density, then integrated over the height and averaged. The equations assume a shallow body of water, therefore the velocity in the z direction is approximately zero. The full calculations are included in the appendix, but the result of these calculations are given in Equations 10 and Equation 11.

$$\frac{\partial \bar{u} H}{\partial t} + \frac{\partial \bar{u}^2 H}{\partial x} + \frac{\partial \bar{u}\bar{v} H}{\partial y} = -\frac{\partial \frac{1}{2} g H^2}{\partial x} \tag{10}$$

$$\frac{\partial \bar{v} H}{\partial t} + \frac{\partial \bar{u}\bar{v} H}{\partial x} + \frac{\partial \bar{v}^2 H}{\partial y} = -\frac{\partial \frac{1}{2} g H^2}{\partial y} \tag{11}$$

Vector notation condenses the three equations into the form:

$$\vec{K} = \begin{pmatrix} H \\ uH \\ vH \end{pmatrix} \tag{12a}$$

$$\vec{F} = \begin{pmatrix} uH \\ u^2 H + \frac{1}{2} g H^2 \\ uvH \end{pmatrix} \tag{12b}$$

$$\vec{G} = \begin{pmatrix} vH \\ uvH \\ v^2 H + \frac{1}{2} g H^2 \end{pmatrix} \tag{12c}$$

(12d)

$$\frac{\partial \vec{K}}{\partial t} + \frac{\partial \vec{F}}{\partial x} + \frac{\partial \vec{G}}{\partial y} = 0 \tag{12e}$$

This final form is then implemented in the MATLAB simulation using the Lax-Wendroff method, which is discussed in later sections.

3 One Dimensional Shallow Water Equations

From the two dimensional shallow water equations it follows that the the one dimensional shallow water equations are given by:

$$\frac{\delta h}{\delta t} + \frac{\delta hv}{\delta x} = 0 \tag{13a}$$

$$\frac{\delta hv}{\delta t} + \frac{\delta}{\delta x}\left(hv^2 + \frac{1}{2} g h^2\right) = -gh\frac{\delta b}{\delta x} \tag{13b}$$

When an uneven bathymetry is introduced (i.e., $\nabla b \neq 0$) a forcing term appears in the conservation of momentum equation, $-gh\frac{b}{x}$. Changing variables to $\begin{pmatrix} H \\ V \end{pmatrix} = \begin{pmatrix} h \\ hv \end{pmatrix}$ yields the equations in the form in which the time derivatives of the two dependant variables are easily isolated.

$$\frac{\delta H}{\delta t} = -\frac{\delta V}{\delta x} \tag{14a}$$

$$\frac{\delta V}{\delta t} = -\frac{\delta}{\delta x}\left(\frac{V^2}{H} + \frac{1}{2} g H^2\right) - gH\frac{\delta b}{\delta x} \tag{14b}$$

Isolating these time derivatives drastically simplifies the implementation of most numerical methods. Solutions to the initial value problem can be approximated with Euler's method, or a variation thereof, over an arbitrarily large domain and for any bathymetry.

4 Shock Waves

4.1 General Definition

Shock waves are defined as discontinuities in physical properties such as temperature, pressure, velocity or density. They are caused when a series of waves overtakes one another, forming a moving boundary that separates the fast and slow moving fluids. This is commonly seen in supersonic flow and when the sound barrier is broken; the air waves compress together into a region of fast moving air that pushes against the slower air around it. The wave front in air is extremely thin, and is usually considered analytically as a jump discontinuity in physical properties.

In shallow water, shock waves occur when waves build up into one higher, steeper wave. This phenomenon is seen with ocean waves as they approach the shore. Since each wave moves independently of the others, the faster waves catch up to and overtake the slower ones, creating the wave front. Additionally, the crests of the waves move more quickly than the bases, which cause ocean waves to "break" or curl over as shown in Figure 3. The discontinuity in this case is in the velocities of the wave and the surrounding water. A shock wave occurs when the ratio of the wave's slope and its height is greater than or equal to one.

4.2 Mathematical Definition

Mathematically, a shock wave is a specific case of the solution to nonlinear hyperbolic partial differential equations, shown in the general case in Equation 15. We will look at a more specific equation, Equation 16, which is the simplest form of the equation for the basic motion of fluids. Despite being nonlinear, this equation can be analyzed using the geometric method, giving the relationship $\frac{dx}{dt} = u(x,t)$. Therefore, each solution has a different set of

characteristic curves whose slopes depend on the solution itself. This property is due to the non-linearity of the equation. Each characteristic curve is also a unique solution for any given point (x_0, t_0) that lies on the curve.

$$u_t + a(u)u_x = 0 \tag{15}$$

$$u_t + uu_x = 0 \tag{16}$$

From Equation 17, we can determine that the time derivative of $u(x,t)$ is zero and that $u(x,t)$ is a constant along each characteristic curve. Hence, each characteristic curve is actually a straight line with a slope equivalent to the value of the solution along that line. Every solution $u(x,t)$ has a family of characteristic lines with various slopes.

$$\frac{d}{dt}[u(x(t),t)] = u_t + \frac{dx}{dt}u_x = u_t + uu_x = 0 \tag{17}$$

Unfortunately, since the lines have different slopes, there is the possibility of having two characteristic lines cross. This would allow a point (x,t) at that intersection to have two possible solutions which violates the uniqueness of the equation. For example, consider a solution with initial condition $u(x,0) = \phi(x)$. At a point $(x_0, 0)$, the characteristic line has a slope of $\phi(x_0)$. However, at a different point $(x_1, 0)$ the characteristic line will have a different slope $\phi(x_1)$ and since the slopes are different the lines will intersect (Figure 2).

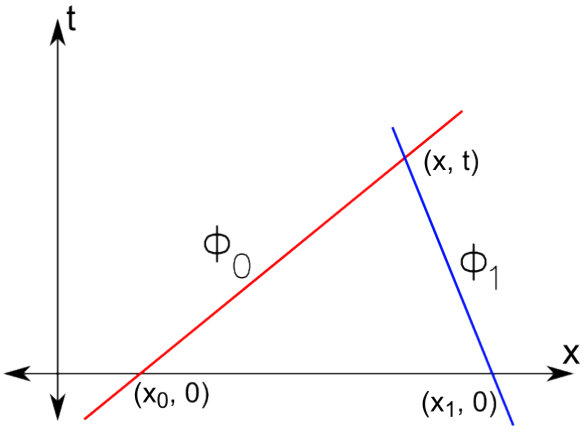

Fig. 2. Example of characteristic lines of different slopes crossing.

To avoid this issue, there are three different approaches that can be taken. The first is to limit the domain to positive values of t whenever the function $\phi(x)$ is increasing for all values of x. This prevents any characteristic lines from intersecting at all. Another possibility is to admit that the solution is only valid near $t = 0$ and that the solution breaks down in unexpected ways as one goes further away from the initial point.

The final option is to allow the solution to contain discontinuities where an intersection would occur. This is the origin of shock wave theory. The solution can only exist in the region up to the time of intersection, and at that intersection the shock wave front occurs. As the solution approaches the intersection, the wave speed is dependent on the value of that solution. In waves, this means that the different parts of the wave travel at different speeds, and eventually the faster moving regions overtake the slower moving regions (Figure 3).

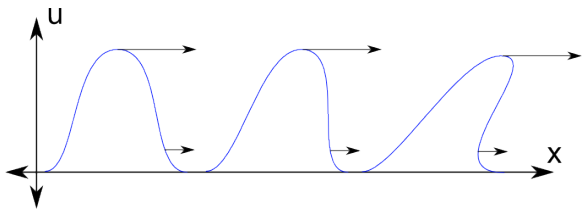

Fig. 3. Different wave regions traveling at different speeds.

This solution also applies to the general form of the equation, Equation 15. The characteristic curves are given by solutions to Equation 18, and we can once again observe the relationship shown in Equation 19. This shows that the characteristic curves of the general equation are in fact straight lines and the solution is constant along those lines.

$$\frac{dx}{dt} = a(u(x,t)) \tag{18}$$

$$\frac{d}{dt}u(x(t),t) = u_x\frac{dx}{dt} + u_t = u_x a(u) - a(u)u_x = 0 \tag{19}$$

If the general equation is solved with the initial condition $u(z,0) = \phi(z)$, assuming the characteristic lines do not intersect, the slope of

the characteristic line for that initial condition can be found (Equation 20). The relationship between ϕ, x, z, and t implies that z is a function of both x and t, yielding the relationship in Equation 21.

$$\frac{x-z}{t-0} = \frac{dx}{dt} = a(u(x,t)) = a(u(z,0)) = a(\phi(z)) \tag{20}$$

$$u(x,t) = u(z,0) = \phi(z) = \phi(z(x,t)) \tag{21}$$

Taking the approach where the solutions are limited to the half plane $t > 0$, the slope must increase with the intercept. Therefore, in order for the characteristic lines not to intersect, $a(\phi(z)) \leq a(\phi(w))$ for $z \leq w$. This means that the lines spread out with distance, creating what is known as a rarefaction or expansive wave. If we were to take the approach where jump discontinuities are allowed in the solution, we would have compression waves that turn into shock waves.

4.2.1 Working with Discontinuous Solutions

Since the solution to Equation 15 is not continuous if the characteristic lines intersect, we can only calculate the weak solutions. This means that the equation needs to be valid in the sense of distributions; it must satisfy Equation 22, where $A'(u) = a(u)$ and $u_t + A(u)_x = 0$ for all $t > 0$.

$$\int_0^\infty \int_{-\infty}^\infty [u\psi_t + A(u)\psi_x] dx dt = 0 \tag{22}$$

We assume that the shock occurs along the curve $x = \xi(t)$ as a jump discontinuity, and the solution is smooth elsewhere. The limits to either side of the jump exist and are $u^+(t) = u(x+,t)$ and $u^-(t) = u(x-,t)$. The speed of the shock is the derivative of the curve, $s(t) = \frac{d\xi}{dt}$. The distribution equation, Equation 22, can be split into sections on either side of the jump discontinuity. Applying the divergence theorem results in Equation 23, where (n_x, n_t) is the unit normal vector to the shock curve that points to the left. Since $u_t + A(u)_x = 0$ from the original definition, the double integrals equal zero leaving Equation 24. Finally, ψ is an arbitrary function and can be canceled from both sides to yield Equation 25. This equation is also known as the Rankine-Hugoniot formula for the speed of a shock wave.

$$\begin{aligned} &\int_0^\infty \int_{-\infty}^{\xi(t)} [-u_t\psi - A(u)_x\psi] dx dt \\ &- \int_{x=\xi(t)} [u^+\psi n_t + A(u^+)\psi n_x] dl \\ &+ \int_0^\infty \int_{\xi(t)}^{+\infty)} [-u_t\psi + A(u)_x\psi] dx dt \\ &+ \int_{x=\xi(t)} [u^-\psi n_t + A(u^-)\psi n_x] dl = 0 \end{aligned} \tag{23}$$

$$\begin{aligned} &\int_{x=\xi(t)} [u^+\psi n_t + A(u^+)\psi n_x] dl \\ &= \int_{x=\xi(t)} [u^-\psi n_t + A(u^-)\psi n_x] dl \end{aligned} \tag{24}$$

$$\frac{A(u^+) - A(u^-)}{u^+ - u^-} = -\frac{n_t}{n_x} = s(t) \tag{25}$$

5 Numerical Methods

Because of the nonlinear nature of the shallow water equations there are few limits in which analytical solutions can be found. Solving the shallow water equations on an arbitrary domain with arbitrary initial data and arbitrary boundary conditions is a task best suited for a computer. To do this the differential equations must be rewritten in a form that can be understood and processed by a computer.

At least one variable, if not all, in the partial differential equation must be discretized. If the partial differential equation can be written in terms of a set of basis functions not all variables must necessarily be discretized. This is not the case for the initial value problem of the arbitrarily bounded shallow water equations, however. In the case of these equations, each variable, spatial and temporal, must be discretized. There are several frameworks to do this, among them are the finite difference method and the finite element method. Both of these methods can be implemented using a variety of different

numerical schemes. Different schemes can be better suited to different problems and some can be more accurate or more computationally expensive than others.

Finite differences differ from finite elements in the method of discretization (see Figure 4). Using a finite difference method the domain over which the equation is being solved is divided into a finite rectangular grid, "finite differences", and the solution is computed at each of the nodes in this grid. Finite elements are similar to finite differences but are not necessarily rectangular rather they can be any polygon; the finite difference method is often considered a special case of the finite element method. Often the domain is triangulated when using a finite element method and the solution is computed at the nodes of this grid. Finite elements also complicate the differential equations because the elements are not organized in an orthogonal grid, confusing the notion of a partial derivative. This method usually requires one or more changes of variables at each of the nodes in order to compensate for the irregular grid pattern. In order to reduce the complexity of this analysis, and because information storage is simpler in a rectangular grid, finite differences have been used to approximate solutions to the shallow water equations.

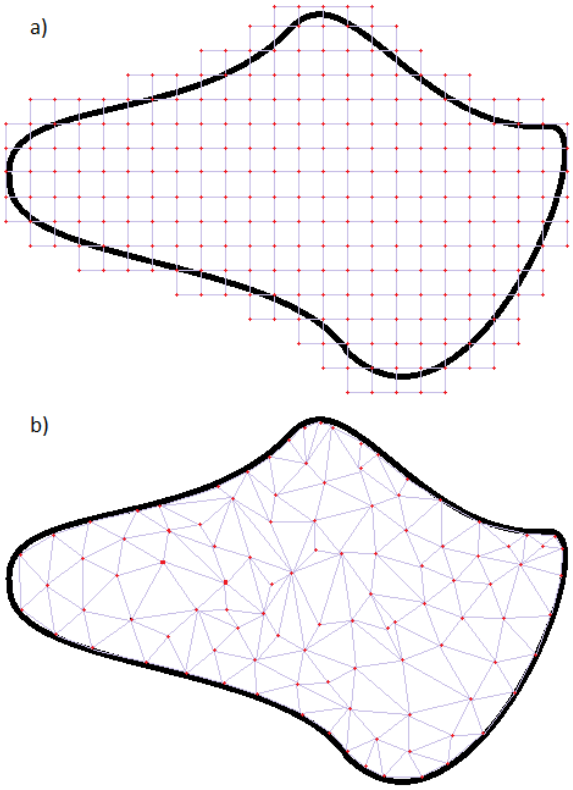

Fig. 4. Illustration of the discretization schemes used by (a) a finite difference method and (b) a finite element method. Finite differences simplify calculations by using a regular rectangular grid. Finite elements involve more complicated calculations, because the grid is neither necessarily rectangular nor regular. Finite elements tend to be more accurate, however because they approximate the boundaries better and they allow for higher resolution where necessary.

5.1 Finite Differences

Finite difference schemes are constructed by relating a function and its derivatives using a Taylor series expansion. The most famous finite difference scheme is Euler's method, which is used to approximate the value of a function of a single variable. In fact Euler's method is simply the repeated use of the first order Taylor series approximation of a function $f(x)$:

$$f(x + \Delta x) \approx f(x) + f'(x)\Delta x \tag{26}$$

Euler's method is considered a first order approximation because it employs the use of the first order Taylor expansion. Higher order approximations employ higher order Taylor series expansions or divide each step into multiple smaller steps (e.g., Runge-Kutte methods). To approximate functions of multiple variables, as will be necessary to develop numerical schemes to solve partial differential equations, the notion of Taylor series is extended to functions of several variables. As with any computation, adding complexity increases the processing time. Higher order approximations of functions of multiple variables, therefore, can be extremely computationally taxing.

Because we are interested in solutions to the shallow water equations on a bounded spatial domain but on a temporal domain with no upper bound (i.e. $t > 0$), rather then creating another grid dimension for the temporal variable, a grid is set up for the spatial variables and is updated as solutions are computed in

the time dimension.

Two finite difference methods to approximate solutions to the shallow water equations were considered here. One method was developed as an extension of Euler's method in several variables. Another method, known as the Lax-Wendroff method, involves dividing the time step into two smaller steps making it a second order approximation in time. The accuracy and expense of computation for each method is compared here.

5.1.1 Notation

Before developing a numerical scheme to approximate solutions to the partial differential equations notation should be established to refer to each node in the finite difference grid. These nodes can be expressed in integer multiples of the difference size. More specifically the coordinate, (x, y), of each node can be given by $(i\Delta x, j\Delta y)$. Similarly, the time variable can be expressed as an integer multiple of the time step, $t = n\Delta t$. In order to condense notation let $f(\vec{x}, t) = f(\vec{i}\Delta\vec{x}, n\Delta t) = f_{\vec{i}}^{n}$.

5.2 Extended Euler Method

The Taylor series expansion applied to functions of several variables can be achieved by using partial derivatives in lieu of ordinary derivatives. This is done by applying the partial derivatives to each variable in sequence and iteratively revising the approximation. For example to approximate a function $f(x, y)$ using a first order Taylor series expansion, the function is first expanded around x:

$$f(x + \Delta x, y) \approx f(x, y) + \frac{\delta f(x, y)}{\delta x}\Delta x \tag{27}$$

or in more concise notation:

$$f_{i+1,j} \approx f_{i,j} + \frac{\delta f_{i,j}}{\delta x}\Delta x \tag{28}$$

This function is then expanded around y:

$$f_{i+1,j+1} \approx f_{i+1,j} + \frac{\delta f_{i+1,j}}{\delta y}\Delta y \tag{29a}$$

$$f_{i+1,j+1} \approx f_{i,j} + \frac{\delta f_{i,j}}{\delta x}\Delta x + \frac{\delta f_{i,j}}{\delta y}\Delta y + \frac{\delta^2 f_{i,j}}{\delta y \delta x}\Delta y \Delta x \tag{29b}$$

Because Δx and Δy are arbitrary this approximation can be used for any point local to (x, y). Often the last term is considered a second order term because it contains two derivatives. Because Δx and Δy are usually small, the term $\Delta x \Delta y$ can be ignored (i.e. $\Delta x < 1$ and $\Delta y < 1 \therefore \Delta x \Delta y \ll 1$).

To solve the initial value problem of a partial differential equation of the form

$$\frac{\delta f(x, t)}{\delta t} = \frac{\delta g(f(x, t))}{\delta x} \tag{30}$$

using the extended Euler method, a difference equation must be obtained that isolates f_*^{n+1} and contains partial derivatives only with respect to the spatial variable, x. The Taylor series of f and g are expanded and rearranged:

$$f_i^{n+1} = f_i^n + \frac{\delta f_i^n}{\delta t}\Delta t \tag{31}$$

$$g_{i+1}^n = g_i^n + \frac{\delta g_i^n}{\delta x}\Delta x \tag{32a}$$

$$\frac{\delta g_i^n}{\delta x} = \frac{g_{i+1}^n - g_i^n}{\Delta x} \tag{32b}$$

Using the partial differential equation, Equation 30, these equations are combined yielding:

$$f_i^{n+1} = f_i^n + \left(g_{i+1}^n - g_i^n\right)\frac{\Delta t}{\Delta x} \tag{33}$$

This is the first-order extended Euler scheme for solving this partial differential equation.

5.2.1 Shallow Water Equations

If instead the partial differential equation is in the form:

$$\frac{\delta \vec{f}(x, y, t)}{\delta t} = \frac{\delta \vec{g}(x, y, t)}{\delta x} + \frac{\delta \vec{h}(x, y, t)}{\delta y} \tag{34}$$

The numerical scheme becomes:

$$f_{i,j}^{n+1} = f_{i,j}^n + \left(g_{i+1,j}^n - g_{i,j}^n\right)\frac{\Delta t}{\Delta x} + \left(h_{i,j+1}^n - h_i^n\right)\frac{\Delta t}{\Delta y} \tag{35}$$

This scheme is conventiently applied to the shallow water equations:

$$\vec{f} = \begin{pmatrix} H \\ U \\ V \end{pmatrix}$$

$$\vec{g} = -\begin{pmatrix} U \\ \frac{U^2}{H} + \frac{1}{2}gH^2 \\ \frac{UV}{H} \end{pmatrix}$$

$$\vec{h} = -\begin{pmatrix} V \\ \frac{UV}{H} \\ \frac{V^2}{H} + \frac{1}{2}gH^2 \end{pmatrix}$$

Where H is the height function, U is proportional to the x component of the momentum field of the water (hu) and V is proportional to the y component of the momentum field of the water (hv).

5.3 Lax-Wendroff Method

Cleve Moler developed a numerical simulation in MATLAB to model shallow water waves using a Lax-Wendroff scheme, which yields a second order approximation to the initial value problem of the the shallow water equations in time and first order in each of the spatial dimensions. Moler's simulation approximates solutions to the two dimensional shallow water equations on a square (see Figure 5). Due credit should be given here to Mr. Moler for developing the architecture of the simulation and for the choice of the Lax-Wendroff scheme to approximate solutions to the shallow water equations. The source code for this simulation has been modified to include the influence of a variable bottom topography and more irregular boundaries and boundary conditions as well as to include the effect of wind across the surface of the water. The numerical scheme was also slightly modified for our purposes. The program architecture and the source code that plotted the data and formatted the image was preserved.

Modifying the boundaries allowed the simulation to run on any path-connected domain with rectangular boundaries, i.e., boundaries with vertical and horizontal normal vectors, including those with obstacles. One of the difference between the simple connected square domain that Moler implemented and the more arbitrary path-connected domain is that the path-connected domain allows for the possibility of inner boundaries, or holes in the domain (see Figure 6). This allows, for example, the simulation of islands in a lake.

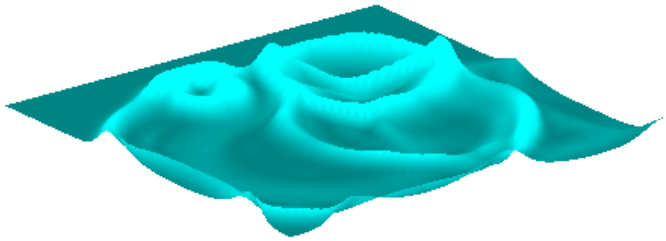

Fig. 5. Numerical solution to an initial value problem of the shallow water equations using an adaptation of Moler's MATLAB simulation.

The one dimensional Lax-Wendroff scheme allows approximations to partial differential equations in the form of Equation 30. The general formulae that constitute the one dimensional Lax-Wendroff method are:

$$\frac{2f_{i+1/2}^{n+1/2} - f_i^n - f_{i+1}^n}{\Delta t} = \frac{g_{i+1}^n - g_i^n}{\Delta x} \tag{36a}$$

$$\frac{f_i^{n+1} - f_i^n}{\Delta t} = \frac{g_{i+1/2}^{n+1/2} - g_{i-1/2}^{n+1/2}}{\Delta x} \tag{36b}$$

These can be derived from first order Taylor series approximations for f and g. To obtain Equation 36a we look at the first order Taylor expansion for $f(x,t)$ in x for a step size of $\frac{\Delta x}{2}$:

$$f_{i+1/2}^n \approx f_i^n + \frac{\delta f_i^n}{\delta x}\frac{\Delta x}{2} \tag{37}$$

Repeating this process for the time variable gives:

$$f_{i+1/2}^{n+1/2} \approx f_i^n + \frac{\delta f_i^n}{\delta x}\frac{\Delta x}{2} + \frac{\delta f_i^n}{\delta t}\frac{\Delta t}{2} + \frac{\delta^2 f_i^n}{\delta t \delta x}\frac{\Delta t \Delta x}{4} \tag{38}$$

As the grid size becomes very small (i.e., $\Delta x \ll 1$ and $\Delta t \ll 1$), the last term vanishes. To solve the initial value problem for partial differential equations in the form of Equation 30, it is sufficient to know the intial data for f. We wish to construct an equation that depends only on f at time $n\Delta t$, i.e., not on $\frac{\delta f}{\delta t}$ and not on f_*^{n+1} or $f_*^{n+1/2}$. Subtracting Equation 37

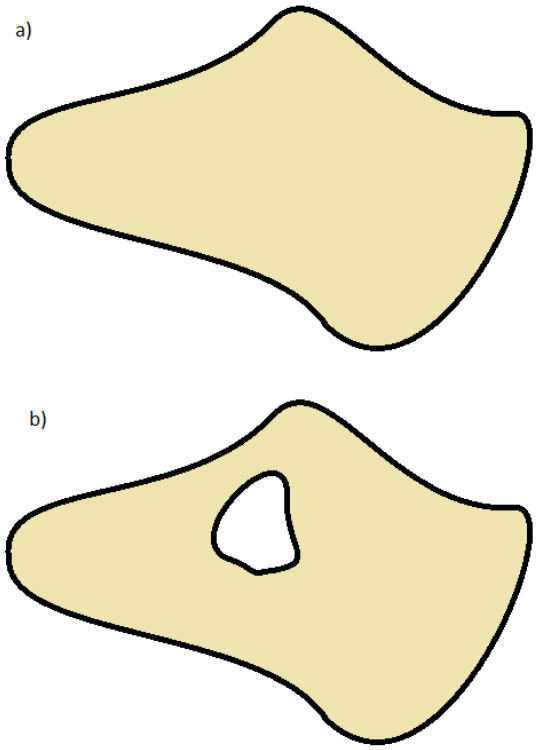

Fig. 6. Illustration of a simply connected domain and a path connected domain. The simply connected domain (a) has one continuous boundary; any two points in the space are connected and any path between these points can be continuously transformed into any other path. The path connected space (b) has more than one continuous boundary; any two points in this space can be connected by a path, but not all paths can be achieved by continuously transforming a single path.

from Equation 38 allows us to isolate the time derivative leaving:

$$\frac{\delta f_i^n}{\delta t} \approx \frac{2\left(f_{i+1/2}^{n+1/2} - f_{i+1/2}^n\right)}{\Delta t} \tag{39}$$

Substituting in Equation 37 gives:

$$\frac{\delta f_i^n}{\delta t} \approx \frac{2\left(f_{i+1/2}^{n+1/2} - f_i^n - \frac{\delta f_i^n}{\delta x}\frac{\Delta x}{2}\right)}{\Delta t} \tag{40}$$

The spatial derivative can be approximated using the first order taylor approximation with a time step Δx:

$$\frac{\delta f_i^n}{\delta x} \approx \frac{f_{i+1}^n - f_i^n}{\Delta x} \tag{41}$$

Using this substitution, Equation 40 becomes:

$$\frac{\delta f_i^n}{\delta t} \approx \frac{2f_{i+1/2}^{n+1/2} - f_i^n - f_{1+i}^n}{\Delta t} \tag{42}$$

By Equation 41 it follows that $\frac{\delta g}{\delta x}$ is the right hand side of Equation 36a. Equation 36b is calculated using a technique similar to Equation 41, but with a centered derivative approximation. Equations 36a and 36b are simply discretized versions of Equation 30.

When these equations are rearranged so that the left hand side is given only in terms of data that is known at each time step they yeild:

$$f_{i+1/2}^{n+1/2} = \frac{f_i^n + f_{i+1}^n}{2} + \left(g_{i+1}^n - g_i^n\right)\frac{\Delta t}{2\Delta x} \tag{43a}$$

$$f_i^{n+1} = f_i^n + \left(g_{i+1/2}^{n+1/2} - g_{i-1/2}^{n+1/2}\right)\frac{\Delta t}{\Delta x} \tag{43b}$$

Equation 43a advances the system one half-timestep forwards, it is given in terms of f_i^n and g_i^n and provides a value for $f_{i+1/2}^{n+1/2}$. Because g is a function of f, this allows $g_{i+1/2}^{n+1/2}$ to be calculated as well. Equation 43b advances the system the rest of the timestep forward, using data from the previous time step and the previous half-timestep.

5.3.1 Shallow Water Equations

If instead the partial differential equation is in the form of Equation 34, the Lax-Wendroff scheme becomes:

$$f_{i+1/2,j}^{n+1/2} = \frac{f_{i,j}^n + f_{i+1,j}^n}{2} + \left(g_{i+1,j}^n - g_i^n\right)\frac{\Delta t}{2\Delta x} \tag{44a}$$

$$f_{i,j+1/2}^{n+1/2} = \frac{f_{i,j}^n + f_{i,j+1}^n}{2} + \left(g_{i,j+1}^n - g_i^n\right)\frac{\Delta t}{2\Delta x} \tag{44b}$$

$$f_{i,j}^{n+1} = f_{i,j}^n + \left(g_{i+1/2,j}^{n+1/2} - g_{i-1/2,j}^{n+1/2} + g_{i,j+1/2}^{n+1/2} - g_{i,j-1/2}^{n+1/2}\right)\frac{\Delta t}{2\Delta x} \tag{44c}$$

This numerical scheme is applied to the shallow water equations in an identical manner to the extended Euler method.

In addition to being a second order approximation to the shallow water equation, making it inherently more accurate than the extended Euler method, the Lax-Wendroff scheme is fast enough to be graphed in real time, producing a dynamic "movie" of a breaking dam using a 25,000 cell grid.

5.4 Reflections

There are three types of boundary conditions that can be dealt with by the simulation: reflective boundary conditions, transparent boundary conditions and dissipative boundary conditions. These boundary conditions are enforced by reserving a single-element buffer space in the matrix (or array, in the one-dimensional case) that extends past the boundary. This buffer space is directly manipulated by the simulation to enforce homogeneous Dirichlet boundary conditions, with an odd reflection, Neumann boundary conditions, with an even reflection, or Robin boundary conditions.

Reflective boundary conditions enforce free (homogeneous Neumann) boundary conditions on height and the velocity component that is travelling parallel to the boundary while enforcing Dirichlet boundary conditions on the velocity component that is travelling perpendicular to the boundaries. Dissipative boundary conditions, similarly, keep the height and the component of the velocity parallel to the boundary free, but use Robin boundary conditions to dissipate energy from the velocity perpendicular to the boundaries. Transparent boundary conditions use homogeneous Neumann boundary conditions for all quantities.

These boundary conditions cause an incoming wave to behave appropriately when they collide with the boundaries at the cost of a single-element space that isn't actually part of the domain. The buffer space poses no problem along the outer boundaries of a domain because they simply just aren't shown when plotting results. However, the buffer space means that internal boundaries can't occupy a single line inside the domain but instead must take up no less than two cells at the obstacle's narrowest point.

A problem arises when our two-dimensional simulator tries to enforce boundary conditions that aren't strictly vertical or horizontal, as illustrated by Figure 7. The expected reflection can be seen on the left side of the figure: a wave (dark blue) comes into the boundary (red) and is reflected off (light blue) at an angle from normal relative to the boundary that is equal to the incident angle of the wave. However, when the simulator models the non- vertical or horizontal boundary on a grid, it turns into many horizontal and vertical boundaries. This causes the error seen in the right side of the figure; an incident wave reflects back on itself off of many small horizontal or vertical segments instead of exiting with an angle equal to the angle of incidence. The short-term solution has been to keep all of our boundaries either vertical or horizontal while we work on creating boundaries that know the local slope so that waves can reflect off of a rectangular grid in a non-rectangular manner.

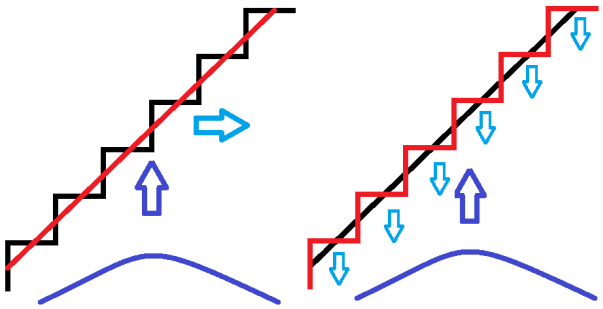

Fig. 7. Illustration of the boundary slope approximation problem. The appropriate reflection (left) cannot be approximated on a grid of rectangular boundaries regardless of the grid resolution.

5.5 Bathymetry

We have developed a simulation to find numerical approximations to solutions of the one-dimensional shallow water equations with non-constant bathymetry.

We have observed an interesting phenomenon as water waves move toward shallower water. Figure 8 illustrates the result of a simulated water wave as it moves across an inclined terrain. As the wave approaches shore, the spatial frequency of the constituent waves grow and the wavefront begins to approximate a step function. This depicts a shortcoming in the shallow water assumption for situations with steep bathymetry. Steep bathymetry slows the wave, allowing the wavefront to

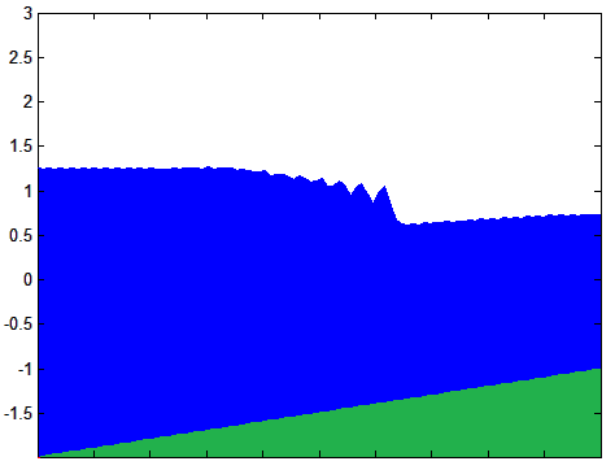

Fig. 8. Illustration of the one dimensional implementation of the initial value problem with bottom terrain. As the wave approaches the shore the wavefront grows and the wave crests.

accumulate. The wavelengths of the constituent waves also shorten, breaking the shallow water assumption. In reality a wave of this nature will break as it approaches the shore, but the shallow water equations are not equipped to describe this phenomenon.

Although this variable bathymetry has been implemented in the one dimensional case, it still needs to be implemented in the two dimensional simulation.

6 Simulation of a Dam Break

The work we have presented so far can be compiled to create a reasonably realitic model of a body of water. These bodies need not simply be things like lakes and rivers, but can be more complex systems like dams and the surrounding areas. We will study the effects of a dam break on a system comprised of an inlet river to the dam and a large spillway on the other side by examining properties like the flow rate of water through the compromised dam and the height of the waves that reach the shoreline. In this manner we will be able to assess damages caused by varying initial conditions such as dam height, size, and amount of water flowing into and out of the system.

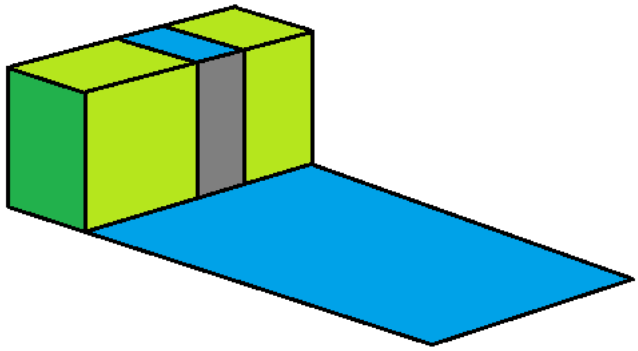

Fig. 9. A visualization of the dam system in question.

6.1 The System

The dam is one third the width of the domain, has a thickness of zero, and the inlet behind it is half the width of the domain in length. On either side of the inlet are regions outside of the domain, creating a situation where a narrow inlet drains into a much larger spillway. We have not yet implemented bathymetry into the dam simulation, so the bottom elevation is entirely at $h = 0$. Additionally, the spillway has a constant height of 2 and the inlet has a constant height of 3. These conditions can be observed in Figure 12 which shows the system at time $t = 0.40$, immediately after the dam has disappeared.

6.2 Effects of the Break

Once the dam is removed, the edge of the inlet closest to the spillway immediately begins falling and creates waves in the spillway. The inlet empties from the spillway side to the edge of the domain, but there reaches a point around $t = 11$ (Figure 13) where the water begins to drain effectively back-to-front; the edge of the inlet against the boundary of the domain falls below the neutral level while the edge of the inlet against the spillway remains higher than the neutral level. Figure 13 also shows the beginning of the formation of vortices near the corners of the dam. These form when the reflection of the wave off of the sides of the domain meets the flow of water that is entering the spillway through the dam. The water

begins to move in circles, as can be seen by looking at the velocity vectors of the water around the areas where the vortices form. (This is something that we would like to examine in future work.) Approximately ten seconds later, at $t = 21.12$, (Figure 14) the primary flood wave has moved out of the domain on its path down the spillway. The inlet is almost entirely emptied, and is beginning to fill back up. This draw of water also pulls the vortices in from the corners of the dam towards the center of the domain until they are both within the width of the inlet. At this point, it would appear that the presence of these two vortices causes the water at the interface between the inlet and the spillway to begin rotating as well, spawning two new vortices inside the inlet. (Figure 15).

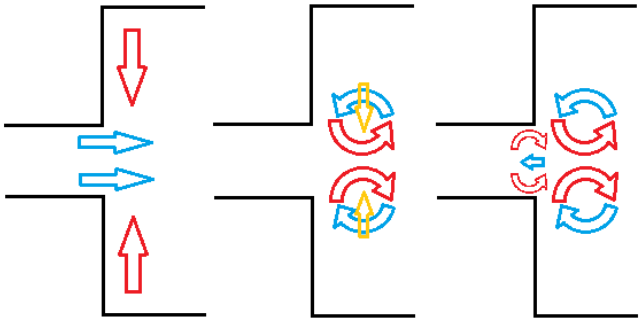

Fig. 10. Sequence of vortex formation.

The water that rushed back into the inlet reflects off of the boundary of the domain and a second surge is produced. This secondary surge is much milder than the primary surge, with the most notable effect being that it pushes two of the vortices away from the mouth of the inlet. (Figure 16) The water equilibrates as time goes on, with the only disturbance being the remains of two of the vortices inside the inlet channel. Inside the area of the spillway, the water remains mostly flat since almost all of the energy has been dissipated through the transparent boundary.

6.3 Flow Rate across the Dam Mouth

A plot of the flow rate against time is shown in Figure 11. This confirms what was observed in the simulation regarding the draining and subsequent refilling of the inlet channel; the flow is positive from $t = 0$ to $t \approx 20$ and then dips negative from $t \approx 20$ to $t \approx 42$ before going positive again.

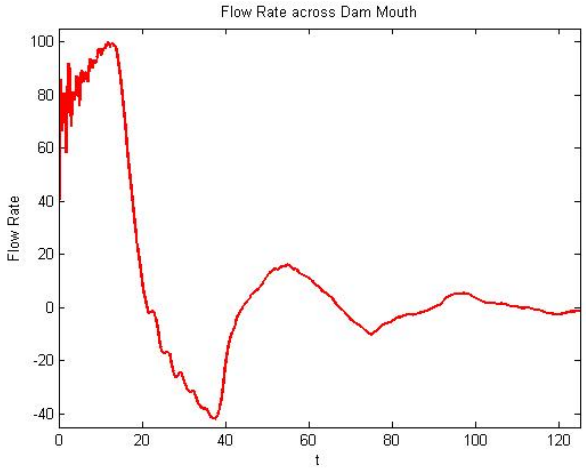

Fig. 11. Flow rate from t = 0 to t = 125. From t = 125 to t = 300, the flow rate is essentially zero.

Another interesting point to note is that the maximum flow rate is achieved not at the beginning of the primary wave but after some time has gone by. This maximum corresponds to the time when the domain boundary side of the inlet reaches a minimum and the rest of the water rushes out of the inlet. The maximum flow does not, however, correspond to the largest amplitude flood wave produced, but instead appears to correspond with the formation of the vortices next to the dam mouth. We suspect that this extra surge outwards helps to spin up the vortices, but further study is necessary to confirm this theory.

6.4 Flow Rate across Spillway Boundary

The flow rate across the end of the spillway takes on a very similar shape to that of the flow rate across the mouth of the dam. (Figure 18) This is due to the fact that water waves only lose energy on boundaries, and there aren't any boundaries between the mouth of the dam and the end of the spillway. It makes sense then that the plots of the flow rates for each of the two areas in question would be similar. The leading flood wave to reach the end of the spillway causes the initial jump in the flow rate, but

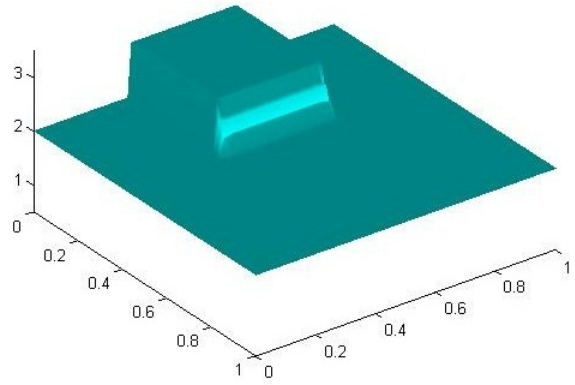

Fig. 12. $t = 0.40$

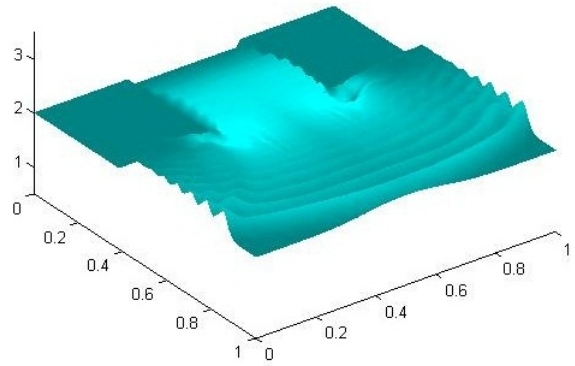

Fig. 13. $t = 11.04$

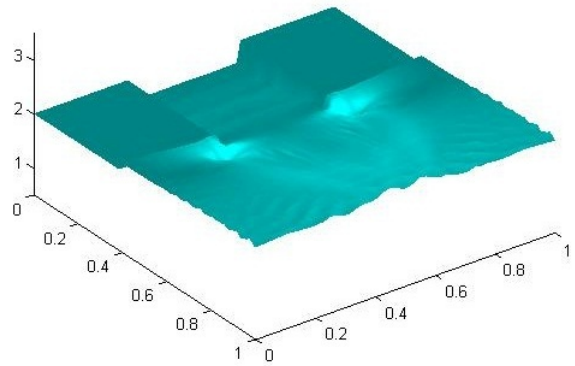

Fig. 14. $t = 21.12$

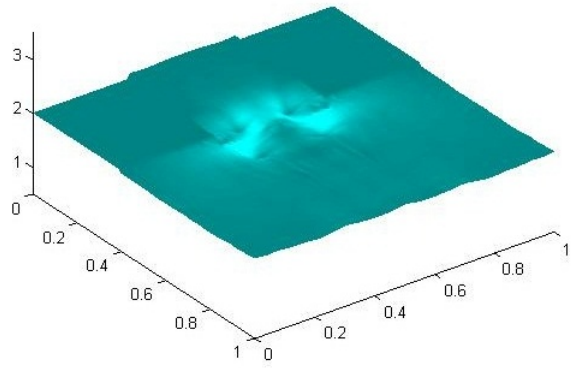

Fig. 15. $t = 39.36$

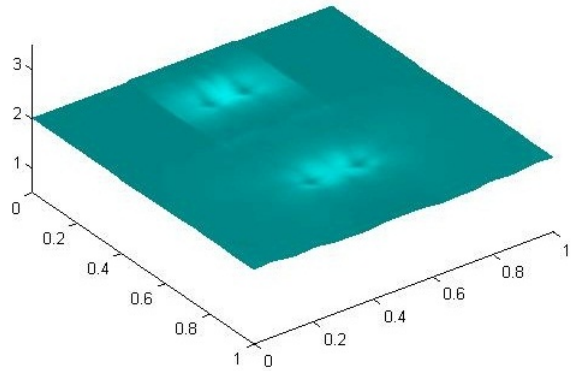

Fig. 16. $t = 90.96$

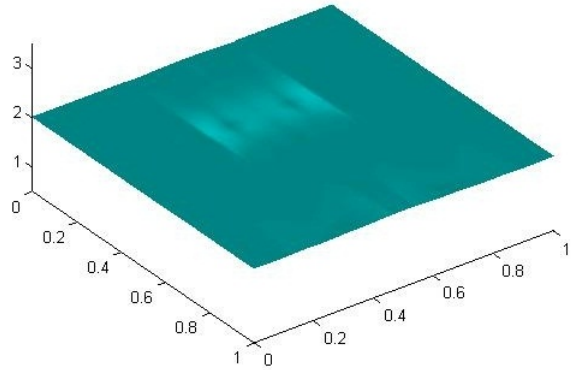

Fig. 17. $t = 300.80$

again the maximum flow rate is reached some time after the first wave reaches the boundary. The same pattern observed at the mouth of the dam follows, where the flow rate drops negative, although not as severely, before going returning positive again.

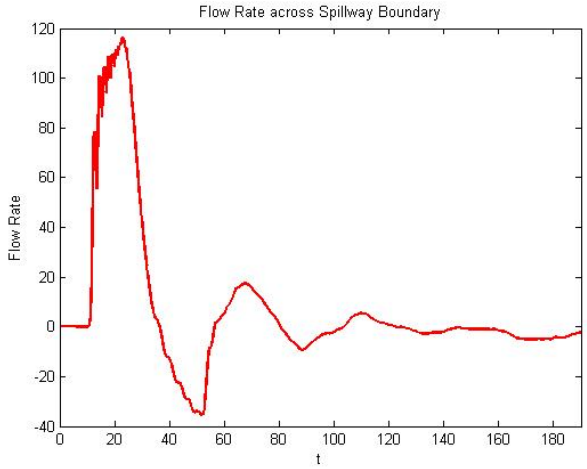

Fig. 18. Flow rate from t = 0 to t = 190. From t = 190 to t = 300, the flow rate is essentially zero. Note the dip when the vorticies cross the edge of the domain at time t = 185.

6.5 Inaccuracies

While the simulation of the dam break can be held to be quite accurate, there is a small source of error that arises from the assumption that we can depth-integrate the z dimension to find the average velocities. As noted earlier, the tops of the waves move faster than the bottoms of the waves which cause them to crest and roll over upon themselves. For small surface waves this is insignificant- there waves are too mild to break and roll over. On the other hand, our dam simulation releases a fairly massive wall of water from the inlet to the spillway, which certainly would be rolling over on itself as it travels down the spillway. As a result, our model overestimates how high the waves are when they reach the shore since cresting would reduce the hight slightly and also how much energy they have upon landfall because the turbulence created would consume some of the energy that the wave is carrying.

7 Effect of Wind on the Shallow Water Equations

7.1 Derivation of Shallow Water Equations with Surface Stress

In our original simulation, we assumed that there was no stress on either the top or bottom surfaces of the water. This is a reasonable assumption, but does not hold if we wish to make the model more realistic by adding wind to the system.

The derivation of the two dimensional shallow water equations with surface stress is similar to the previous shallow water equation derivation, but an extra term is carried throughout the calculations. In this case, the Navier Stokes equations that are used are Equations 45 and 46, which contain the stress tensor term $\nabla \cdot \bar{T}$ that was ignored earlier.

$$\nabla \cdot \vec{v} = 0 \tag{45a}$$

$$\frac{\partial}{\partial t}\rho\vec{v} + \nabla \cdot (\rho\vec{v}\vec{v}) = -\nabla P + \rho\vec{g} + \nabla \cdot \bar{T} \tag{45b}$$

$$\frac{\partial u}{\partial x} + \frac{\partial v}{\partial y} + \frac{\partial w}{\partial z} = 0 \tag{46a}$$

$$\frac{\partial(\rho u)}{\partial t} + \frac{\partial(\rho u^2)}{\partial x} + \frac{\partial(\rho uv)}{\partial y} + \frac{\partial(\rho uw)}{\partial z} = -\frac{\partial P}{\partial x} + \frac{\partial T_{xx}}{\partial x} + \frac{\partial T_{xy}}{\partial y} + \frac{\partial T_{xz}}{\partial z} \tag{46b}$$

$$\frac{\partial(\rho v)}{\partial t} + \frac{\partial(\rho uv)}{\partial x} + \frac{\partial(\rho v^2)}{\partial y} + \frac{\partial(\rho vw)}{\partial z} = -\frac{\partial P}{\partial y} + \frac{\partial T_{xy}}{\partial x} + \frac{\partial T_{yy}}{\partial y} + \frac{\partial T_{yz}}{\partial z} \tag{46c}$$

$$\frac{\partial(\rho w)}{\partial t} + \frac{\partial(\rho uw)}{\partial x} + \frac{\partial(\rho wv)}{\partial y} + \frac{\partial(\rho w^2)}{\partial z} = -\frac{\partial P}{\partial z} - \rho g + \frac{\partial T_{xz}}{\partial x} + \frac{\partial T_{zy}}{\partial y} + \frac{\partial T_{zz}}{\partial z} \tag{46d}$$

The boundary conditions for the system are generally the same, but new conditions must be added for the stress tensor term. At the surface of the water, $z = \zeta$, the surface stress is defined by Equation 47. This stress is usually known, and in the case where the stress is entirely due to wind it can be calculated from the wind

speed. However, the bottom stress, $\bar{T}_b$, is caused by friction and therefore cannot be calculated explicitly. It is defined at $z = -b$ by Equation 48, but its value must be determined by the model.

(at z = ζ)

$$T_{sx} = -T_{xx}\frac{\partial \zeta}{\partial x} - T_{xy}\frac{\partial \zeta}{\partial y} + T_{xz} \tag{47a}$$

$$T_{sy} = -T_{xy}\frac{\partial \zeta}{\partial x} - T_{yy}\frac{\partial \zeta}{\partial y} + T_{yz} \tag{47b}$$

(at z = b)

$$T_{bx} = T_{xx}\frac{\partial b}{\partial x} + T_{xy}\frac{\partial b}{\partial y} + T_{xz} \tag{48a}$$

$$T_{by} = T_{xy}\frac{\partial b}{\partial x} + T_{yy}\frac{\partial b}{\partial y} + T_{yz} \tag{48b}$$

For our simulation we will assume that $\bar{T}_b$, the stress along the bottom of the flow, is negligible. However, the surface stress $\bar{T}_s$ is calculated from Equation 49 using the wind speed, $\vec{W}$, and physical characteristics of the air. The effective stresses, T_{xx}, T_{xy}, and T_{yy}, can be calculated from the fluid velocities and fluid properties, using Equation 50.

$$T_{sx} = C_d \rho_{air} W_x \sqrt{W_x^2 + W_y^2} \tag{49a}$$

$$T_{sy} = C_d \rho_{air} W_y \sqrt{W_x^2 + W_y^2} \tag{49b}$$

$$T_{xx} = \frac{2\rho\nu}{H}\frac{\partial H\bar{u}}{\partial x} \tag{50a}$$

$$T_{yy} = \frac{2\rho\nu}{H}\frac{\partial H\bar{v}}{\partial y} \tag{50b}$$

$$T_{xy} = \frac{\rho\nu}{H}(\frac{\partial H\bar{u}}{\partial y} + \frac{\partial H\bar{v}}{\partial x}) \tag{50c}$$

Since the conservation of mass equation has not changed, those steps of the derivation remain the same. For the momentum equations, we assume that there is no stress in the z component so it is simplified in the same manner as earlier. This once again gives us an equation for pressure which can be differentiated and substituted back into the x and y components. The components are then integrated over the height and multiplied by $\frac{1}{H}$ to give averaged velocities. The left hand sides of the equations are the same as the original derivation. The right hand sides are treated similarly (see Appendix), resulting in Equations 51 and 52. These final equations are implemented in MATLAB following the Lax-Wendroff scheme, just like the original equations.

$$\frac{\partial \bar{u}H}{\partial t} + \frac{\partial \bar{u}^2 H}{\partial x} + \frac{\partial \bar{u}\bar{v}H}{\partial y} = -\frac{\partial \frac{1}{2}gH^2}{\partial x} + \frac{H}{\rho}(T_{sx} - T_{bx}) + \frac{H}{\rho}(\frac{\partial}{\partial x}\int_{-b}^{\zeta} T_{xx}dz + \frac{\partial}{\partial y}\int_{-b}^{\zeta} T_{xy}dz) \tag{51}$$

$$\frac{\partial \bar{v}H}{\partial t} + \frac{\partial \bar{u}\bar{v}H}{\partial x} + \frac{\partial \bar{v}^2 H}{\partial y} = -\frac{\partial \frac{1}{2}gH^2}{\partial y} + \frac{H}{\rho}(T_{sy} - T_{by}) + \frac{H}{\rho}(\frac{\partial}{\partial x}\int_{-b}^{\zeta} T_{xy}dz + \frac{\partial}{\partial y}\int_{-b}^{\zeta} T_{yy}dz) \tag{52}$$

7.2 Effect of Surface Stress on the Simulation

In order to include the stresses in the simulation, the extra terms from the derivation are simply added to the code. The surface stress is constant throughout the simulation, so it is calculated at the beginning of the program using Equation 49. The drag coefficient C_d equals $.001$, which is of the proper order of magnitude since the exact value varies with wind speed. The physical constants were assumed to be $\rho_{air} = 1.25\frac{kg}{m^3}$ and $\nu_{air} = 1.5 * 10^{-5}\frac{m^2}{s}$. The effective stresses depend on the velocity of the fluid, so they had to be calculated within the code itself.

The shallow water equations with wind stress were implemented in both the one and two dimensional cases. For both simulations, the water begins at rest at a uniform height. In one dimension, the wind causes the surface of the water to angle upwards as the water is pushed forward by the flow. In doing so it causes waves to form, which then reflect at the boundaries and pass back and forth along the

domain. The waves move at varying speeds, so they eventually compress together and create a shock wave that dominates the flow (Figure 19 through 22). The same phenomenon is seen in two dimensional flow; the water angles upwards in the direction of the wind and eventually forms waves that compress into a shock wave. However, the change in amplitude of the water surface is more difficult to see in the two dimensional model (Figure 23 through 26). The codes were validated by testing the cases where the wind speed is zero, or is only acting in one dimension. The models acted as expected, showing that at least the qualitative behavior is correct.

December 16, 2011

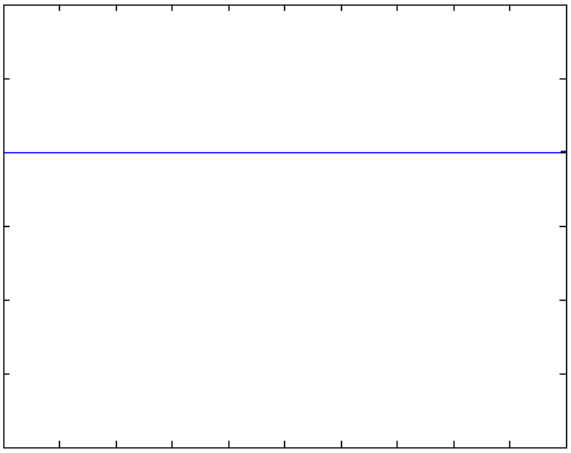

Fig. 19. One dimensional wave with wind of 2 m/s at t = 0.

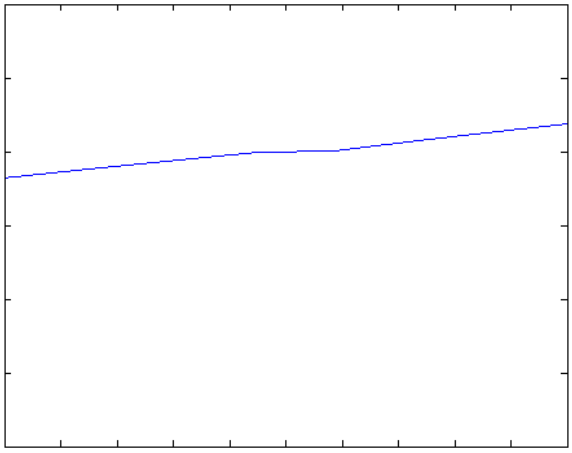

Fig. 20. One dimensional wave with wind of 2 m/s at t = 10.

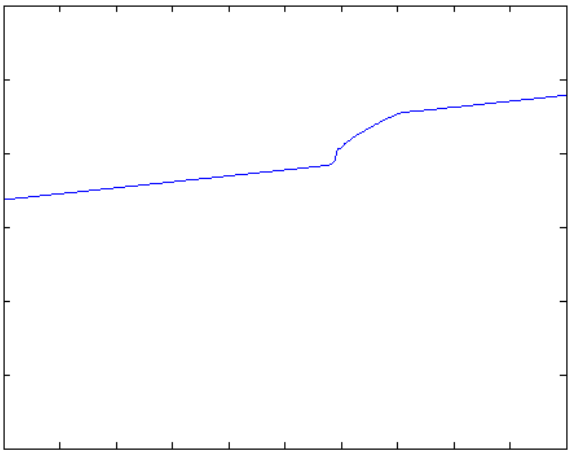

Fig. 21. One dimensional wave with wind of 2 m/s at t = 110.

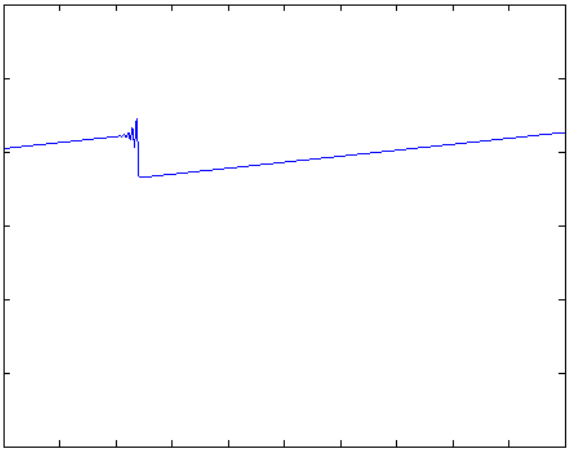

Fig. 22. One dimensional wave with wind of 2 m/s at t = 130.

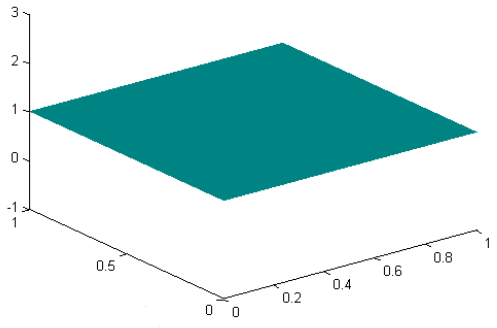

Fig. 23. Two dimensional wave with wind of 4 m/s in both the x and y directions at t=0

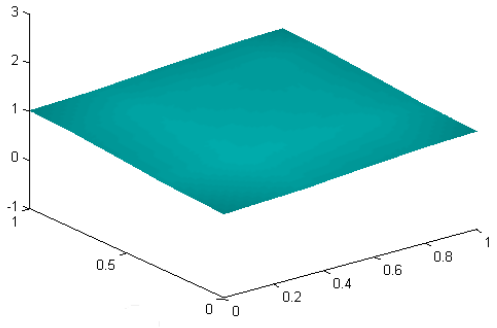

Fig. 24. Two dimensional wave with wind of 4 m/s in both the x and y directions at t=20

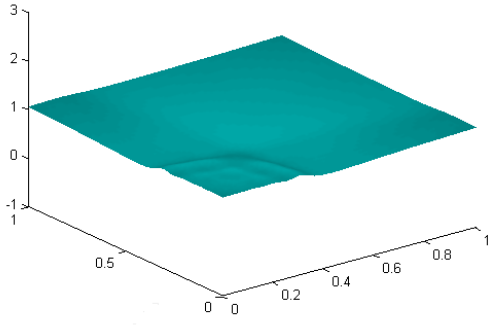

Fig. 25. Two dimensional wave with wind of 4 m/s in both the x and y directions at t=110

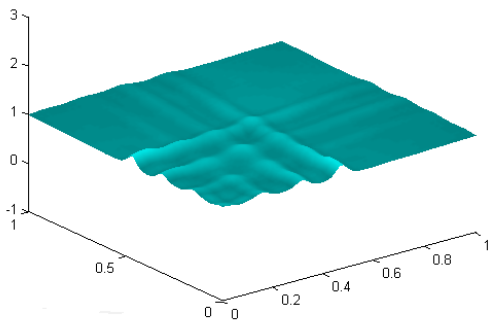

Fig. 26. Two dimensional wave with wind of 4 m/s in both the x and y directions at t=210

APPENDIX A
DETAILED DERIVATION OF THE SHALLOW WATER WAVE EQUATIONS

Begin with the Navier Stoke's Equations in component form

$$\begin{aligned}
\frac{\partial u}{\partial x}+\frac{\partial v}{\partial y}+\frac{\partial w}{\partial z} &= 0\\
\frac{\partial(\rho u)}{\partial t}+\frac{\partial(\rho u^2)}{\partial x}+\frac{\partial(\rho uv)}{\partial y}+\frac{\partial(\rho uw)}{\partial z} &= -\frac{\partial P}{\partial x}\\
\frac{\partial(\rho v)}{\partial t}+\frac{\partial(\rho uv)}{\partial x}+\frac{\partial(\rho v^2)}{\partial y}+\frac{\partial(\rho vw)}{\partial z} &= -\frac{\partial P}{\partial y}\\
\frac{\partial(\rho w)}{\partial t}+\frac{\partial(\rho uw)}{\partial x}+\frac{\partial(\rho wv)}{\partial y}+\frac{\partial(\rho w^2)}{\partial z} &= -\frac{\partial P}{\partial z}-\rho g
\end{aligned}$$

To find the pressure at a given height, assume all velocities are extremely small with respect to the z direction, therefore only the pressure and gravity components of the z direction equation remain.

$$\begin{aligned}
0 &= -\frac{\partial P}{\partial z}+\rho g\\
-\frac{\partial P}{\partial z} &= \rho g\\
\int_z^\zeta -\frac{\partial P}{\partial z}dz &= \int_z^\zeta \rho g dz\\
P|_\zeta - P|_z &= \rho g(z|_z^\zeta)\\
0-P &= \rho g(\zeta - z)\\
P &= \rho g(\zeta - z)
\end{aligned}$$

The equation for conservation of mass is found by integrating the Navier Stoke's equation and converting the result to averages.

$$\begin{aligned}
0 &= \int_{-b}^{\zeta} \nabla\cdot\vec{v}dv\\
0 &= \int_{-b}^{\zeta}(\frac{\partial u}{\partial x}+\frac{\partial v}{\partial y}+\frac{\partial w}{\partial z})dz\\
0 &= \int_{-b}^{\zeta}(\frac{\partial u}{\partial x}+\frac{\partial v}{\partial y})dz + w|_{-b}^{\zeta}
\end{aligned}$$

The Liebniz Rule states:

$$\int_{a(\alpha)}^{b(\alpha)}\frac{d}{d\alpha}f(x,\alpha)dx = f(b(\alpha),\alpha)\frac{db(\alpha)}{d\alpha} - f(a(\alpha),\alpha)\frac{da(\alpha)}{d\alpha} + \int_{a(\alpha)}^{b(\alpha)}\frac{\partial}{\partial\alpha}f(x,\alpha)dx$$

Therefore, the equation becomes

$$0 = \frac{\partial}{\partial x}\int_{-b}^{\zeta} u dz - (u|_\zeta\frac{\partial\zeta}{\partial x}+u|_{-b}\frac{\partial b}{\partial x}) + \frac{\partial}{\partial y}\int_{-b}^{\zeta} v dz - (v|_\zeta\frac{\partial\zeta}{\partial y}+v|_{-b}\frac{\partial b}{\partial y}) + (w|_\zeta - w|_{-b})$$

From boundary conditions, $v = u = w = 0$ at the bottom surface ($z = -b$).

$$0 = \frac{\partial}{\partial x}\int_{-b}^{\zeta} u dz - u|_\zeta\frac{\partial\zeta}{\partial x} + \frac{\partial}{\partial y}\int_{-b}^{\zeta} v dz - v|_\zeta\frac{\partial\zeta}{\partial y} + w|_\zeta$$

The integrals are changed to averages using the equations $\bar{u} = \frac{1}{H}\int_{-b}^{\zeta} u dz$ and $\bar{v} = \frac{1}{H}\int_{-b}^{\zeta} v dz$ then rearranged.

$$\frac{\partial}{\partial x}(\bar{u}H) + \frac{\partial}{\partial y}(\bar{v}H) + (-u\frac{\partial \zeta}{\partial x} - v\frac{\partial \zeta}{\partial y} + w) = 0$$

The expression within the parenthesis, $-u\frac{\partial \zeta}{\partial x} - v\frac{\partial \zeta}{\partial y} + w$ is equivalent to $\frac{\partial \zeta}{\partial t}$ from the boundary conditions. Since the equations are applied in a case where $b = 0$, $H = \zeta$.

$$\frac{\partial H}{\partial t} + \frac{\partial \bar{u}H}{\partial x} + \frac{\partial \bar{v}H}{\partial y} = 0$$

The x and y momentum equations are found using a similar process. In the last step, we assume that $w = 0$ because of the shallowness.

$$\begin{aligned}
\frac{\partial(\rho u)}{\partial t} + \frac{\partial(\rho u^2)}{\partial x} + \frac{\partial(\rho uv)}{\partial y} + \frac{\partial(\rho uw)}{\partial z} &= -\frac{\partial P}{\partial x} \\
\frac{\partial u}{\partial t} + \frac{\partial u^2}{\partial x} + \frac{\partial uv}{\partial y} + \frac{\partial uw}{\partial z} &= -\frac{1}{\rho}\frac{\partial P}{\partial x} \\
\int_{-b}^{\zeta}(\frac{\partial u}{\partial t} + \frac{\partial u^2}{\partial x} + \frac{\partial uv}{\partial y} + \frac{\partial uw}{\partial z})dz &= -\frac{1}{\rho}\int_{-b}^{\zeta}\frac{\partial P}{\partial x}dz \\
\frac{\partial \bar{u}H}{\partial t} + \frac{\partial \bar{u}^2 H}{\partial x} + \frac{\partial \bar{u}\bar{v}H}{\partial y} &= -\frac{1}{\rho}\int_{-b}^{\zeta}\frac{\partial P}{\partial x}dz
\end{aligned}$$

Now we look at the integral on the right side of the equation.

$$\begin{aligned}
&= \int_{-b}^{\zeta}\frac{\partial P}{\partial x}dz \\
&= \int_{-b}^{\zeta}\frac{\partial \rho g(\zeta - z)}{\partial x}dz \\
&= \frac{\partial \rho g(\zeta z - \frac{1}{2}z^2)}{\partial x}\Big|_{-b}^{\zeta} \\
&= \frac{\partial \rho g(\zeta^2 - \frac{1}{2}\zeta^2)}{\partial x} - \frac{\partial \rho g(-\zeta b - \frac{1}{2}\zeta^2)}{\partial x} \\
&= \frac{\partial \rho g(\frac{1}{2}\zeta^2 + \zeta b + \frac{1}{2}b^2)}{\partial x} \\
&= \frac{\partial \frac{1}{2}\rho g(\zeta + b)^2}{\partial x} \\
&= \frac{\partial \frac{1}{2}\rho g(H)^2}{\partial x} \\
&= \rho\frac{\partial \frac{1}{2}gH^2}{\partial x}
\end{aligned}$$

Combining this with the left side of the equation yields the final expression.

$$\frac{\partial \bar{u}H}{\partial t} + \frac{\partial \bar{u}^2 H}{\partial x} + \frac{\partial \bar{u}\bar{v}H}{\partial y} = -\frac{\partial \frac{1}{2}gH^2}{\partial x}$$

The same process is then repeated with the y momentum equation.

$$\frac{\partial \bar{v}H}{\partial t} + \frac{\partial \bar{u}\bar{v}H}{\partial x} + \frac{\partial \bar{v}^2 H}{\partial y} = -\frac{\partial \frac{1}{2}gH^2}{\partial y}$$

A.1 Detailed Derivation of the Shallow Water Equations with Surface Stress

The derivation for the shallow water equation with surface stress is extremely similar to the derivation without surface stress. The main difference is in including the stress terms while integrating the right hand side of the momentum equations. The Leibniz rule is used since the boundary conditions change with position, but the overall calculation is straightforward. The steps for the x momentum calculations are shown below; the y momentum calculations are similar.

$$
\begin{aligned}
&= \int_{-b}^{\zeta} (\frac{\partial P}{\partial x} + \frac{\partial T_{xx}}{\partial x} + \frac{\partial T_{xy}}{\partial y} + \frac{\partial T_{xz}}{\partial z}) dz \\
&= \int_{-b}^{\zeta} (-\rho g \frac{\partial \zeta}{\partial x} + \frac{\partial T_{xx}}{\partial x} + \frac{\partial T_{xy}}{\partial y} + \frac{\partial T_{xz}}{\partial z}) dz \\
&= -\rho g \frac{\partial \zeta}{\partial x} z|_{-b}^{\zeta} + (\int_{-b}^{\zeta} \frac{\partial T_{xx}}{\partial x} dz + \frac{\partial \zeta}{\partial x} T_{xx} - \frac{\partial b}{\partial x} T_{xx}) \\
&+ (\int_{-b}^{\zeta} \frac{\partial T_{xy}}{\partial y} dz + \frac{\partial \zeta}{\partial y} T_{xy} - \frac{\partial b}{\partial y} T_{xy}) + \int_{-b}^{\zeta} \frac{\partial T_{xz}}{\partial z} dz
\end{aligned}
$$

From the boundary conditions, the terms can be condensed into the surface and bottom stresses. This expression is then combined with the left hand side of the equation to yield the full equation.

(at z = ζ)

$$T_{sx} = -T_{xx} \frac{\partial \zeta}{\partial x} - T_{xy} \frac{\partial \zeta}{\partial y} + T_{xz}$$

(at z = b)

$$T_{bx} = T_{xx} \frac{\partial b}{\partial x} + T_{xy} \frac{\partial b}{\partial y} + T_{xz}$$

$$= -\rho g \tfrac{\partial \zeta}{\partial x} (\zeta + b) + (T_{sx} - T_{bx}) + \int_{-b}^{\zeta} \tfrac{\partial T_{xx}}{\partial x} dz + \int_{-b}^{\zeta} \tfrac{\partial T_{xy}}{\partial y} dz$$

REFERENCES

[1] Beffa, Cornel. "2D-Shallow Water Equations: Basics, Solutions, Applications." . N.p., Dec 2008. Web. 30 Nov 2011. <http: //www.ifu.ethz.ch/GWH/education/graduate/ Hydraulik_II/Vorlesungen/k8_EN.pdf>.
This source provided a look at deriving the shallow water equations and some approaches to solving them with numerical solvers.

[2] Burkardt, John . Virginia Tech, 03.02.2010. Web. <http: //people.sc.fsu.edu/ jburkardt/presentations/ shallow_water_2010.pdf>.
This source provided an in-depth explanation of the shallow water equations and also a detailed explanation of the Lax-Wendroff method implemented by the numerical solver.

[3] Mirabito, Christopher M. , and Clint Dawson. University of Texas at Austin, 09.29.2008. Web. <http: //users.ices.utexas.edu/ arbogast/cam397/dawson_v2.pdf>.
This source provided a derivation of the shallow water equations that included how to take bathymetry data and stress tensors from the wind blowing across the surface of the water into account.

[4] Moler, Cleve. MathWorks, 10.02.2011. Web. <http: //www.mathworks.com/moler/exm/chapters/water.pdf>
This source provided an introduction into the shallow water equations but more importantly provided the original source code which we modified to create our numerical solver.

[5] Peregrine, D.H.. "Water Waves and their Development in Space and Time". 07.08.1985. <http: //www.jstor.org/stable/pdfplus/2397595.pdf?acceptTC=true>.
This source provided additional information about the conditions surrounding breaking waves.

[6] Pratt, L. J. , and John A. Whitehead. *Rotating Hydraulics: Nonlinear Topographic Effects in the Ocean and Atmosphere*. 2007.
This source provided detailed information and calculations regarding non-linear steepening and the formation of shock waves in water.

[7] Strauss, Walter A.. *Partial Differential Equations: An Introduction*. 1992.
This source provided information about the formation of shock waves and the related mathematical calculations

[8] Zhou, J. G , D. M. Causon, D. M. Ingram and C. G. Mingham. "Numerical solutions of the shallow water equations with discontinuous bed topography". The Manchester Metropolitan University. 2002. <http: //www.see.ed.ac.uk/ dingram/publications/Zhou02.pdf>.
This source provided an explanation of how to implement and calculate the stresses acting on a fluid in two dimensions.